

See discussions, stats, and author profiles for this publication at: <https://www.researchgate.net/publication/229662882>

The Global Symplectic Integrator: An efficient tool for stability studies of dynamical systems. Application to the Kozai resonance in the restricted three-body problem

Article in *Monthly Notices of the Royal Astronomical Society* · March 2011

DOI: 10.1111/j.1365-2966.2011.18431.x

CITATIONS

4

3 authors:



Anne-Sophie Libert

University of Namur

66 PUBLICATIONS 851 CITATIONS

[SEE PROFILE](#)

READS

381



Charles Hubaux

8 PUBLICATIONS 98 CITATIONS

[SEE PROFILE](#)



Timoteo Carletti

University of Namur

220 PUBLICATIONS 2,137 CITATIONS

[SEE PROFILE](#)

Some of the authors of this publication are also working on these related projects:



Space Debris [View project](#)



Optimization in the large [View project](#)

The Global Symplectic Integrator: an efficient tool for stability studies of dynamical systems. Application to the Kozai resonance in the restricted three-body problem

A.-S. Libert,[★] Ch. Hubaux[★] and T. Carletti[★]

Namur Center for Complex Systems (NAXYS) Department of Mathematics FUNDP, 8 Rempart de la Vierge, B-5000 Namur, Belgium

Accepted 2011 January 26. Received 2011 January 24; in original form 2010 November 12

ABSTRACT

Following the discovery of extrasolar systems, the study of long-term evolution and stability of planetary systems is enjoying a renewed interest. While non-symplectic integrators are very time-consuming because of the very long time-scales and the small integration steps required to have a good energy preservation, symplectic integrators are well suited for the study of such orbits on long time-spans. However, stability studies of dynamical systems generally rely on non-symplectic integrations of deviation vectors. In this work we propose a numerical approach to distinguish between regular and chaotic orbits in Hamiltonian systems, hereby called *Global Symplectic Integrator*. It consists of the simultaneous integration of the orbit and the deviation vectors using a symplectic scheme of any order. In particular, due to its symplectic properties, the proposed method allows us to recover the correct orbit characteristics using very large integration time-steps, fluctuations of energy around a constant value and short CPU times. It proves to be more efficient than non-symplectic schemes to correctly identify the behaviour of a given orbit, especially on dynamics acting on long time-scales. To illustrate the numerical performances of the global symplectic integrator, we will apply it to the well-known toy problem of Hénon–Heiles and the challenging problem of the Kozai resonance in the restricted three-body problem, whose secular effects have periods of the order of 10^4 – 10^5 yr.

Key words: methods: numerical – planets and satellites: dynamical evolution and stability – planetary systems.

1 INTRODUCTION

To date, ~ 50 extrasolar multiplanetary systems have been detected. The determination of the stability of these planetary systems is a major issue in celestial mechanics. Indeed, although these systems are generally believed to be on nearly coplanar orbits (due to both the limitations of the currently available detection techniques and the general expectation that planetary systems are similar to the Solar system), the results of McArthur et al. (2010) for the ν Andromedae system have shown that the orbital planes of planets c and d of this system probably have a mutual inclination of $\sim 30^\circ$. The possibility of such a stable 3D configuration has been previously highlighted by some analytical studies, namely Michtchenko, Ferraz-Mello & Beaugé (2006), Libert & Henrard (2007, 2008), Libert & Tsiganis (2009), where it has been shown that planetary systems with more than two planets on highly mutually inclined orbits can

be long-term stable, either following regular secular dynamics or due to the action of some phase-protection mechanism, such as a mean motion resonance (MMR) or a secular Kozai-type resonance (Kozai 1962). In particular, Libert & Tsiganis (2009) found that four two-planet extrasolar systems (ν Andromedae, HD 12661, HD 169830 and HD 74156) have orbital parameters consistent with a stable Kozai-resonant state, if their (unknown) mutual inclination is $\sim 45^\circ$.

Long-term stability studies are also required in the search of potential additional terrestrial planets inside the habitable zone of extrasolar planetary systems (e.g. Menou & Tabachnik 2003; Sándor et al. 2007; Funk et al. 2008, 2011). In particular, Funk et al. (2011) performed a parametric study showing the impact of an outer gas giant on the dynamics of the fictitious planet, for various mutual inclinations between their orbital planes. Again, the influence of the Kozai mechanism on the stability of the test-planet is obvious and investigated in detail in Funk et al. (2011).

In the aforementioned N -body problems, the Kozai resonance is acting on particularly long time-scales, as its secular effects have periods of the order of 10^4 – 10^5 yr (Libert & Henrard 2007). From

[★]E-mail: anne-sophie.libert@fundp.ac.be (A-SL); charles.hubaux@fundp.ac.be (ChH); timoteo.carletti@fundp.ac.be (TC)

the computational point of view, the problem of distinguishing between regular and chaotic behaviors affected by secular resonances is really challenging: it requires the integration of the evolution of deviation vectors with a sufficiently small time-step (~ 1 d) for a sufficiently long integration time-span (at least 10^6 yr). While the usual non-symplectic algorithms are generally efficient for instabilities generated by mean-motion resonances between the bodies, whose effects appear on quite short time-scales, they reveal to be poor indicators of the secular instabilities in N -body problems (e.g. Funk et al. 2011). As a result, the aim of the present contribution is the introduction of an efficient tool for stability studies on very long time-scales.

Hamiltonian systems exhibit phase spaces where regular and chaotic orbits do coexist. This fact makes the problem of the numerical characterization of regular and chaotic motion a hard task, notably in systems with many degrees of freedom. For this reason, scientists developed fast and accurate tools to obtain information about the chaotic versus regular nature of the orbits of such systems, and efficiently characterize large domains in their phase space as ordered or (weakly) chaotic.

These methods can be roughly divided into two major groups. The first group consists of the *Lyapunov-like* methods i.e. methods based on the study of the evolution of deviation vectors for a given orbit; the methods FLI (Froeschlé, Lega & Gonczi 1997), MEGNO (Cincotta & Simó 2000), SALI (Skokos 2001) and GALI (Skokos, Bountis & Antonopoulos 2007). The second group consists of *Fourier-like* methods based on the determination of the frequencies of the spectrum of some observable related to a given orbit, for instance FMA (Laskar, Froeschlé & Celletti 1992; Laskar 1993) or the spectral method (Guzzo & Benettin 2001). In the present work we are interested in the former group or class of methods, in particular the SALI chaos detection technique.

To numerically compute such an indicator, one needs to have a good orbit determination, but one also needs to integrate the evolution of two deviation vectors. It is well known that symplectic integration schemes of the equations of motion outperform non-symplectic ones, when compared using the same order of accuracy and the same integration step size. This is mainly due to the very good energy conservation properties of these schemes, and also due to other first integrals. As a consequence, larger step sizes are allowed while still keeping a reasonably small energy loss. Thus they allow us to enlarge considerably the time-span of the numerical simulation, without degrading the goodness of the numerical results. That is why symplectic integrators turn out to be essential for the long-term evolution of a dynamical system, and are widely used in the study of the long-term evolution of N -body problems [e.g. SWIFT (Wisdom & Holman 1991; Levison & Duncan 1994), SYMBA (Duncan, Levison & Lee 1998), MERCURY (Chambers & Migliorini 1997)].

In the same way, chaos detection techniques could also benefit from the use of symplectic integrators. The aim of the present work is to show that the symplectic integration of the deviation vectors can improve the ability of the previous chaos indicators in the characterization of regular and chaotic orbits by correctly identifying the orbit behaviour, using a larger integration step size. Because our method proposes to integrate simultaneously both the orbit and the deviation vectors, using a symplectic scheme, we hereby name this method *Global Symplectic Integrator*.

Let us note that the symplectic integration of the deviation vectors (or equivalently the tangent map) has already been discussed in the literature (e.g. Mikkola & Innanen 1999; Guzzo 2005), but generally the algorithm is introduced for a specific problem and the variational

equations are derived by performing a derivative of the symplectic scheme used, hence the method relies on a specified order of the used symplectic integrator (usually the second-order Leap Frog integrator). Our present work aims to be more general in the sense that the Global Symplectic Integrator is suitable for a large class of Hamiltonian systems, whatever the order of the used symplectic integrator.

The performances of our symplectic method will be straightforwardly emphasized on a toy model, the classical Hénon–Heiles system. More precisely, we will accurately determine, using a symplectic scheme and a small enough integration time-step, the characteristics, i.e. the regular or chaotic behaviour, of a large number of orbits using the SALI chaos detectors. Then, all the previous orbits will be reanalyzed using both symplectic and non-symplectic integrator schemes, but with larger and larger time-steps. We will show that the use of the global symplectic integrator will allow us to recover a large percentage of orbits characteristics with very large time-steps compared to the non-symplectic one and using a small amount of CPU time.

Finally, our Global Symplectic Integrator also turns out to be essential for multidimensional problems, like the study of the long-term evolution of planetary systems. This will be shown in the case of Kozai-resonant systems in the restricted three-body problem, for which the possibility of using large integration step sizes saves a considerable amount of CPU time.

The paper is organized as follows. In Section 2, we describe our method for integrating symplectically the deviation vectors used in the chaos detection techniques. For the sake of completeness, we present, in Section 3, a brief introduction to the SALI chaos indicator. Our method is validated on the Hénon–Heiles system in Section 4, while Section 5 is devoted to its application to the Kozai resonance in the restricted three-body problem. Finally, our conclusions are given in Section 6.

2 THE METHOD

Let us consider a generic Hamiltonian vector field,

$$\dot{\mathbf{x}} = \mathbf{J} \nabla_{\mathbf{x}} H(\mathbf{x}), \quad (1)$$

where $\mathbf{x} = (\mathbf{p}, \mathbf{q}) \in \mathbb{R}^{2n}$ is the momentum-position vector in the phase space, $H(\mathbf{x})$ is the Hamilton function describing the system and $\mathbf{J} = \begin{pmatrix} 0_n & -1_n \\ 1_n & 0_n \end{pmatrix}$ is the standard constant symplectic matrix. The solution of (1) with initial datum \mathbf{x}_0 can be formally written as

$$\varphi(t) = e^{tL_H} \mathbf{x}_0, \quad (2)$$

where L_H is the Lie operator, i.e. for all smooth function defined in the phase space we have $L_H f = \{H, f\}$, being $\{ \cdot, \cdot \}$ the Poisson bracket.

Given a deviation vector \mathbf{v} , its time evolution is described by the tangent map:

$$\frac{d\mathbf{v}}{dt} = \mathbf{M}(\varphi(t)) \mathbf{v}, \quad (3)$$

where \mathbf{M} is the Jacobian of the Hamiltonian vector field (1), namely $\mathbf{M} = \mathbf{J} \nabla_{\mathbf{x}}^2 H$, evaluated on the solution $\varphi(t)$.

Because $\nabla_{\mathbf{x}}^2 H$ is a symmetric matrix, the matrix \mathbf{M} is a Hamiltonian one i.e. $\mathbf{M}^T \mathbf{J} + \mathbf{J} \mathbf{M} = 0$. Hence also the vector field (3) is Hamiltonian, with Hamiltonian function

$$K(\mathbf{v}) = \frac{1}{2} \mathbf{v}^T \mathbf{S} \mathbf{v}, \quad (4)$$

where $\mathbf{S} = \nabla_{\mathbf{x}}^2 H$.

The evolution of a deviation vector could be obtained by the simultaneous integration of the equations of motion (1) and the variational equations (3) with any non-symplectic algorithm. However, for very long time stability analysis, a symplectic scheme may be preferred due to its very good energy conservation properties. In the following, we show that, for a Hamiltonian function H which may be split into two separately integrable parts, the simultaneous integration of both systems (1) and (3) is always possible in a symplectic way.

Let us now assume that the function H can be decomposed into the sum of two parts, each one separately integrable, for instance each one depending only on one group of variables¹

$$H(\mathbf{x}) = A(\mathbf{p}) + B(\mathbf{q}). \quad (5)$$

Let us observe that in the case of the restricted three-body problem (see Section 5), we will prefer to use a different splitting of the Hamiltonian function: actually the function A will correspond to two non-interacting two-body problems that in rectangular coordinates will thus result in a function of positions and momenta; while the remainder will be by definition the B function.

Under the above assumptions, a family of suitable symmetric symplectic schemes has been presented in Laskar & Robutel (2001), hereafter called $SABA_n$. Such methods develop the solution given by (2) using the Baker–Campbell–Hausdorff formula (Bourbaki 1972), allowing the approximation of the true solution by a finite number of compositions of integrable symplectic maps, the error of the approximation being a function of the integration step size τ .

More precisely one can find coefficients $(c_i)_{i=1,\dots,n+1}$ and $(d_i)_{i=1,\dots,n}$ such that the map

$$\begin{aligned} SABA_n(\mathbf{x}) = & e^{c_1 \tau L_A} e^{d_1 \tau L_B} \dots e^{d_n \tau L_B} \\ & \times e^{c_{n+1} \tau L_A} e^{d_n \tau L_B} \dots e^{d_1 \tau L_B} e^{c_1 \tau L_A}(\mathbf{x}) \end{aligned} \quad (6)$$

is symmetric under the transformation $t \mapsto -t$, symplectic and of order $\mathcal{O}(\tau^{2n})$, namely there exists a Hamiltonian function \tilde{H} whose exact flow is given by (6) and moreover $\tilde{H} = H + \mathcal{O}(\tau^{2n})$.

Rewriting the deviation vector as $\mathbf{v} = (\mathbf{v}_p, \mathbf{v}_q)$ i.e. identifying its components with the natural splitting of the phase space, we can explicitly write the Hamiltonian K as follows:

$$K(\mathbf{p}, \mathbf{q}, \mathbf{v}) = \frac{1}{2} \mathbf{v}_p^T \mathcal{A}(\mathbf{p}) \mathbf{v}_p + \frac{1}{2} \mathbf{v}_q^T \mathcal{B}(\mathbf{q}) \mathbf{v}_q, \quad (7)$$

where

$$\mathcal{A}(\mathbf{p}) = \nabla_p^2 A(\mathbf{p}) \quad \text{and} \quad \mathcal{B}(\mathbf{q}) = \nabla_q^2 B(\mathbf{q}). \quad (8)$$

Hence the symmetric symplectic methods $SABA_n$ can be used also to integrate the evolution of the deviation vectors.

The aim of this paper is to show that the use of a symplectic integrator to solve both the orbit evolution and the tangent equation i.e. to get the time evolution of the deviation vector, can improve the capability of some widely used chaos indicators (such as SALI) to determine the characteristics of the orbits in a Hamiltonian system.

Our claim will be numerically proved, for the Hénon–Heiles system, using $SABA_4$ and $SABA_2$ symplectic schemes in comparison with the non-symplectic fourth-order Runge–Kutta method (see Section 4); while $SABA_{10}$ and Bulirsch–Stoer integrators will be used for the study of the restricted three-body problem (see Section 5). In the rest of the paper, the easily implementable SALI chaos

¹ In the meanwhile, Skokos & Gerlach (2010) proposed a symplectic integration scheme for variational equations in the particular case of a Hamiltonian system whose kinetic energy is quadratic in the momenta.

detection technique will be used to numerically determine the orbit characteristics. For the sake of completeness, the next section will be devoted to a brief introduction of this chaos indicator.

3 THE SALI CHAOS INDICATOR

The Smaller ALignment Index, SALI (Skokos 2001), has been proved to be an efficient and simple method to determine the regular or chaotic nature of orbits in conservative dynamical systems. Thanks to its properties, it has been already successfully applied to distinguish between regular and chaotic motion both in symplectic maps and Hamiltonian flows (e.g. Széll et al. 2004; Manos & Athanassoula 2005; Boreux et al. 2010).

For the sake of completeness, let us briefly recall the definition of SALI and its behaviour for regular and chaotic orbits, restricting our attention to symplectic flows. Interested readers can consult Skokos (2001) and Skokos et al. (2004) for a more detailed description of the method. To compute SALI of a given orbit, one has to follow the time evolution of the orbit itself and also of two linearly independent unitary deviation vectors, $\hat{\mathbf{v}}_1(0), \hat{\mathbf{v}}_2(0)$. The evolution of an orbit is given by (2), while the evolution of each deviation vector is given by the tangent map (3).

Then, according to Skokos (2001), SALI for the given orbit is defined by

$$\text{SALI}(t) = \min \{ \| \hat{\mathbf{v}}_1(t) + \hat{\mathbf{v}}_2(t) \|, \| \hat{\mathbf{v}}_1(t) - \hat{\mathbf{v}}_2(t) \| \}, \quad (9)$$

where $\| \cdot \|$ denotes the usual Euclidean norm and $\hat{\mathbf{v}}_i(t) = \frac{\mathbf{v}_i(t)}{\| \mathbf{v}_i(t) \|}$, $i = 1, 2$, are normalized vectors.

In the case of chaotic orbits, the deviation vectors $\hat{\mathbf{v}}_1, \hat{\mathbf{v}}_2$ eventually become aligned in the direction defined by the maximal Lyapunov characteristic exponent (LCE, Benettin et al. 1980), and SALI(t) falls exponentially to zero. An analytical study of SALI's behaviour for chaotic orbits was carried out in Skokos et al. (2004) where it was shown that

$$\text{SALI}(t) \propto e^{-(\sigma_1 - \sigma_2)t}, \quad (10)$$

with σ_1, σ_2 being the two largest LCEs.

In the case of regular motion, on the other hand, the orbit lies on a torus and the vectors $\hat{\mathbf{v}}_1, \hat{\mathbf{v}}_2$ eventually fall on its tangent space, following a t^{-1} time evolution, having in general different directions. In this case, SALI oscillates about non-zero values (for more details see Skokos et al. 2004). This behaviour is due to the fact that for regular orbits the norm of a deviation vector increases linearly in time. Thus, the normalization procedure brings about a decrease in the magnitude of the coordinates perpendicular to the torus at a rate proportional to t^{-1} and so $\hat{\mathbf{v}}_1, \hat{\mathbf{v}}_2$ eventually fall on the tangent space of the torus.

The simplicity of SALI's definition, its completely different behaviour for regular and chaotic orbits and its rapid convergence to zero in the case of chaotic motion are the main advantages that make SALI an ideal chaos detection tool. For all these reasons, the SALI indicator will be used in the following.

The scheme we used to numerically compute SALI consists of integrating both the orbit and the deviation vector using the symmetric symplectic $SABA$ method, and then computing the indicator according to definition (9).

4 VALIDATION OF OUR METHOD: THE HÉNON–HEILES SYSTEM

In this section, we will verify the performances of our Global Symplectic Integrator by considering, as toy problem, the Hénon–Heiles

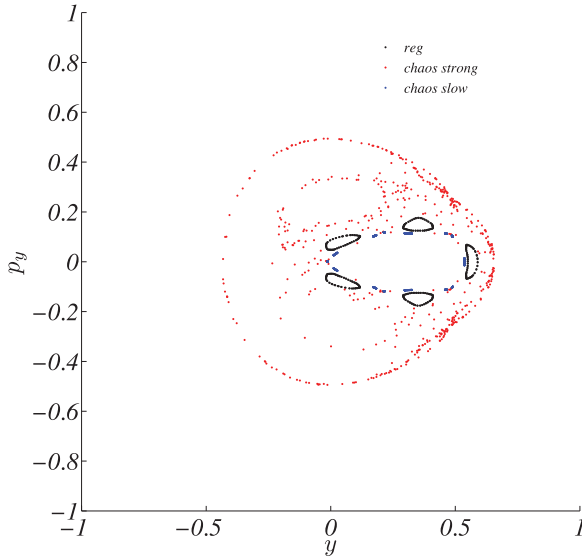


Figure 1. Hénon–Heiles phase space (section $x = 0$). The energy has been fixed to $E = 1/8$ and three characteristic orbits have been computed on this energy level: a regular orbit (black) with initial data $x(0) = 0$, $y(0) = 0.55$, $p_x \sim 0.2417$ and $p_y = 0$, a chaotic orbit strongly diffusing (red) with initial data $x(0) = 0$, $y(0) = -0.016$, $p_x \sim 0.49974$ and $p_y = 0$, and a chaotic orbit slowly diffusing (blue) with initial data $x(0) = 0$, $y(0) = -0.01344$, $p_x \sim 0.49982$ and $p_y = 0$.

system. The analysis of this widely studied dynamical system will point out that chaos indicators can benefit from our method, regarding the characterization of regular and chaotic motion.

The Hénon–Heiles Hamiltonian system (Hénon & Heiles 1964) is a well-known model described by the following Hamilton function:

$$H(p_x, p_y, x, y) = \frac{1}{2} (p_x^2 + p_y^2 + x^2 + y^2) + x^2 y - \frac{1}{3} y^3. \quad (11)$$

In the phase space, regular and chaotic orbits coexist (see the three selected orbits of Fig. 1), whose characteristics can be accurately and rapidly determined with our symplectic scheme presented in the previous sections, using *SABA*₄ integrator with a time-step size $\tau = 10^{-4}$. The choice of a fourth-order integrator is motivated by a balance between reliability and computation time. Indeed, the smaller the used time-step or the higher the integrator order, the better the energy preservation, but the longer the computation time. In this respect, we decided to adopt a *SABA*₄ integrator with the sufficiently small time-step of $\tau = 10^{-4}$.

In Fig. 2, we report the results of the numerical computation of SALI for the three generic orbits of Fig. 1. Since the characteristic period of the orbits on this energy level is of the order of 10 time units, the integration time-span has been fixed to 10^4 time units. We can observe that the three possible dynamical behaviors, regular orbits, chaotic orbits strongly diffusing and chaotic orbits slowly diffusing, are well identified. Let us in fact observe that the strong chaotic behaviour of the red orbit is translated into a quick decrease of SALI to zero. On the contrary, for the black regular orbit, SALI remains bounded away from zero. The blue orbit has a particular behaviour: for quite a long time, up to $\sim 30\,000$ time units, this orbit ‘follows closely’ a periodic, thus regular, orbit, and SALI remains positive, but eventually the chaotic characteristics of the orbit manifest and the indicator correctly goes to zero. Actually the above orbit is close to an unstable periodic orbit.

To check the robustness of our method with respect to a non-symplectic one, first we reanalyzed the above three orbits using

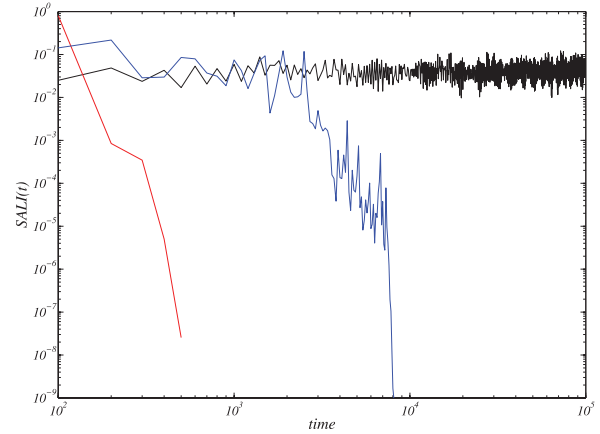


Figure 2. Characterization of the three orbits of Fig. 1: a regular orbit (black), a chaotic orbit strongly diffusing (red) and a chaotic orbit slowly diffusing (blue). The integration step size has been fixed to $\tau = 10^{-4}$ and both the orbit and the deviation vectors have been numerically integrated using the *SABA*₄ method.

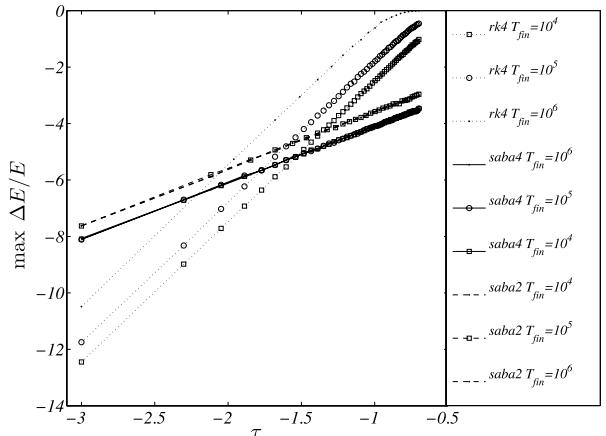


Figure 3. Relative energy loss, $\max_{0 \leq t \leq T_{\text{fin}}} |\Delta E(t)/E(t)|$, for *SABA*₄, *SABA*₂ and *RK4* integrators as a function of the time-steps. Both quantities are given in logarithmic scale. Several integration times are selected, $T_{\text{fin}} = \{10^4, 10^5, 10^6\}$, as given in the legend.

larger time-steps. More precisely, we have numerically computed the SALI indicator using *SABA*₂, *SABA*₄ and *RK4* integrators and time-steps for which the energy loss is bounded by the sufficiently small value 10^{-3} . The time-step values can be easily computed using the results of Fig. 3, where we report the relative energy loss, averaged over 50 randomly chosen orbits, for the integrators *SABA*₄, *SABA*₂ and *RK4*, as a function of the time-steps. For the sake of completeness, we computed the relative energy loss using several integration time-spans. Let us emphasize that the energy losses for symplectic integrators are almost the same for all the integration time-spans for a fixed value of τ , while the non-symplectic scheme *RK4* exhibits a strong dependence on the integration time-span: the larger the time-span, the worst is the energy loss for a fixed value of τ . As expected, the larger the time-step used, the larger the loss of energy. In the following, we fix the largest time-steps, τ , such that the relative energy loss is smaller than 10^{-3} , for an integration time-span equal to 10^4 time units. Under these assumptions we get $\tau_{\text{max}} \sim 0.3$ for *SABA*₄, $\tau_{\text{max}} \sim 0.16$ for *SABA*₂ and $\tau_{\text{max}} \sim 0.08$ for *RK4*. As a result, for the Hénon–Heiles system, our symplectic

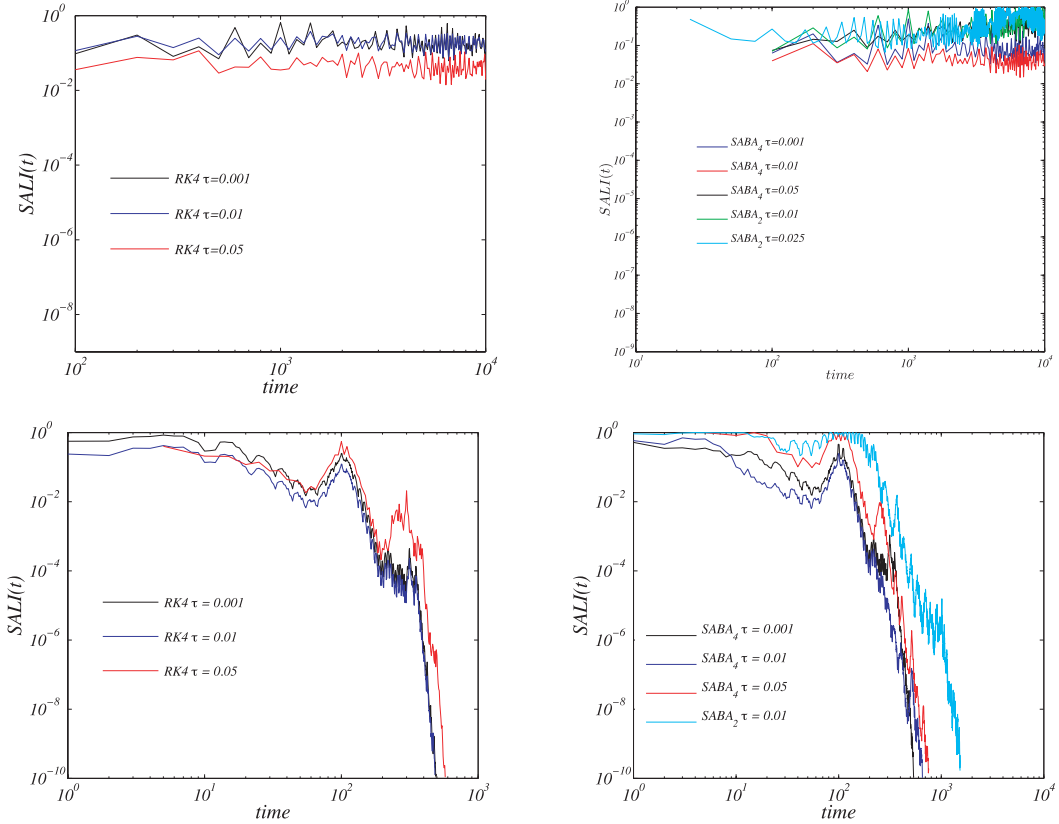


Figure 4. Comparison of integration schemes on the regular orbit $x = 0$, $y = 0.55$, $p_x \sim 0.2417$ and $p_y = 0$ (top panels), and on the chaotic orbit $x = 0$, $y = -0.016$, $p_x \sim 0.49974$ and $p_y = 0$ (bottom panels). Left-hand panels: SALI computed using non-symplectic RK4 for time-steps $\tau \in \{0.001, 0.01, 0.05\}$. Right-hand panels: SALI computed using SABA₄ for the integration of both the orbit and the deviation vectors, for the same time-steps. Both methods determine correctly the characteristics of the orbits independently of the small time-step used.

scheme allows time-steps four times larger than a non-symplectic one of the same order, as will be shown hereafter.

With these maximal realistic time-steps in mind, we reanalyzed the three orbits of Fig. 2 with time-steps $\tau \in \{10^{-3}, 0.01, 0.05\}$ for which the energy loss is small enough, even for the RK4 integrator. All the integration schemes behave almost equally for all the small used time-steps, as it can be observed from the results reported in Fig. 4.

The next step of our comparison is to consider a larger portion of phase space to capture information on the characterization of the global dynamics using symplectic and non-symplectic integration schemes. We hence consider $N_{\text{reg}} = 100$ randomly chosen regular orbits and $N_{\text{cha}} = 100$ randomly chosen chaotic orbits, whose behaviour has been accurately determined using a sufficiently small step size τ , namely $\tau = 10^{-4}$, and a fourth-order symplectic scheme. Then we compute, as a function of the used step size, how many orbits are correctly characterized by the RK4 non-symplectic integration, and by the SABA₂ and SABA₄ symplectic integration for both the orbit and the deviation vectors.

On the one hand, the results reported in Fig. 5 clearly show that, for regular orbits, almost all schemes are able to recover nearly 100 per cent of regular orbits. Concerning the step sizes, Fig. 5 shows that SABA₄ characterizes correctly the dynamics of the same percentage of orbits with four times larger time-steps than RK4, while SABA₂ does the same with two times larger time-steps than RK4, but let us observe that its order is half the one of RK4. On the other hand, the same conclusion holds for the chaotic orbits. Moreover, let us note that there is a general trend of RK4 to overestimate

the number of regular orbits when increasing the time-step. Thus, our symplectic scheme is largely better than RK4 to characterize regular orbits, regarding both the used time-step and the integration order. Indeed, SABA₂ symplectic integrations turn out to be nearly as reliable as the SABA₄ ones, especially for small step sizes.

In Fig. 6 we report the CPU times averaged over 50 randomly chosen orbits, T_{CPU} , as a function of the time-steps. One can clearly see that the symplectic schemes are faster than RK4 using the same step size; more precisely, SABA₄ is almost 2.5 times faster than RK4. Once again this fact illustrates the good numerical performance of our method which is less time consuming in itself, but also allows larger time-steps, again reducing the computational time.

To quantify the *efficiency* of our symplectic scheme, we introduce the following efficiency indicator:

$$\varepsilon = p |\log_{10}(|\Delta E/E|)| |\log_{10}[T_{\text{CPU}}/\max(T_{\text{CPU}})]|, \quad (12)$$

whose dependence as a function of the time-step τ is represented in Fig. 7. Let us observe that the larger the ε , the better the integration scheme. For small integration time-steps, the non-symplectic RK4 scheme dominates, mainly because its energy loss is measly (see Fig. 3), while for time-steps τ larger than 0.03, the situation is reversed: the global symplectic method dominates, as its energy loss and CPU times are both relatively small (see Figs 3 and 6). So the Global Symplectic Integrator proves to be more efficient than the non-symplectic scheme when using large time-steps, which is an asset for the study of very long term dynamics.

As a result, it appears that the use of a symplectic integrator to compute the time evolution of the deviation vectors can improve

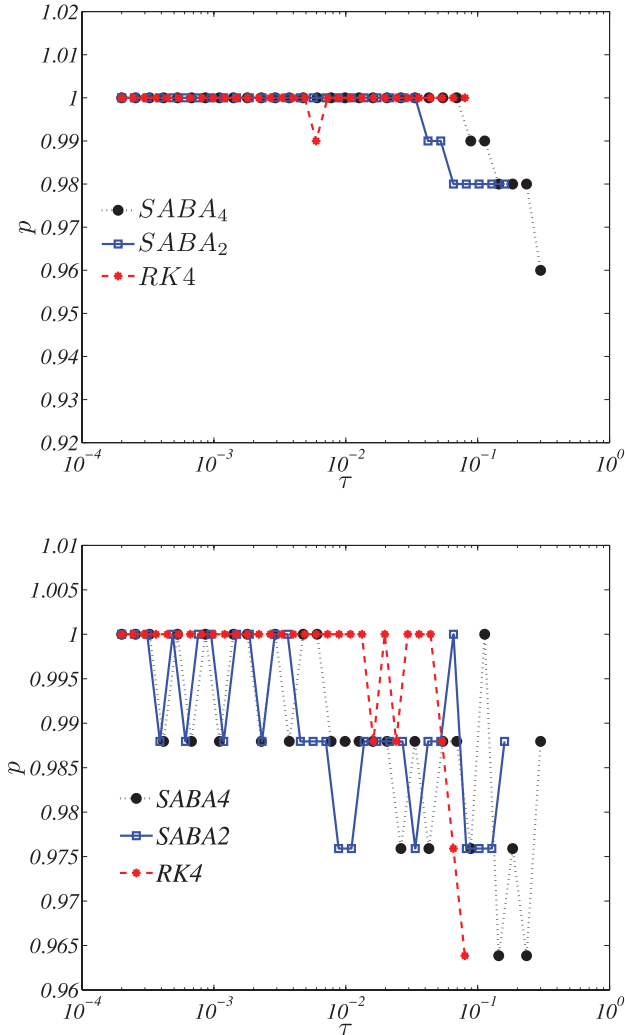


Figure 5. Global comparison between RK4 non-symplectic scheme and SABA₄, SABA₂ symplectic schemes for a large portion of the Hénon–Heiles phase space: $N_{\text{reg}} = 100$ regular orbits and $N_{\text{cha}} = 100$ chaotic orbits are considered. Top panel: percentage of correctly identified regular orbits for increasing time-steps ($p = \text{correctly identified orbits}/\text{total number of orbits}$). Bottom panel: same as top panel for chaotic orbits.

the capability of a chaos indicator such as SALI to determine the characteristics of the orbits of a Hamiltonian system. Furthermore, we have shown that our global symplectic integrator allows larger time-steps without energy loss and saves a considerable amount of computation time. This possibility turns out to be essential for the study of problems of celestial mechanics, where the time-scales are fixed by physical constraints, as for instance in the case of secular resonances in the N -body problem, as will be shown in the next section.

5 RESULTS ON THE KOZAI RESONANCE IN THE RESTRICTED THREE-BODY PROBLEM

The problem of three celestial bodies interacting with each other gravitationally is a well-known problem in celestial mechanics. In the following we will consider the restricted problem. More precisely, one of the bodies, hereafter called the Sun, is the largest mass around which the two other bodies are assumed to evolve; the second body, possessing an intermediate mass and hereafter called Jupiter,

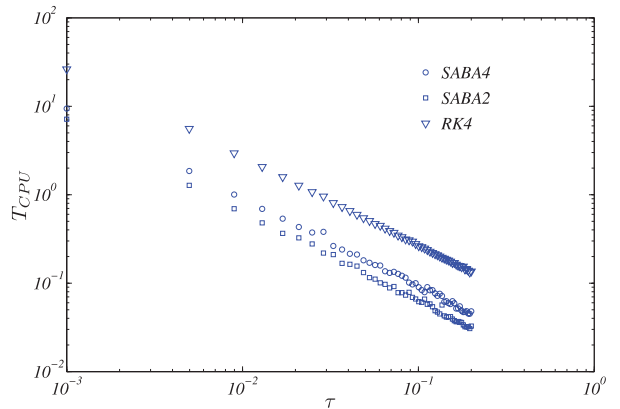


Figure 6. CPU time as a function of the time-step τ . Both quantities are given in logarithmic scale. Linear best fits (data not shown) provide an almost linear decrease in T_{CPU} as a function of τ . The time integration span has been fixed to $T_{\text{fin}} = 10^4$.

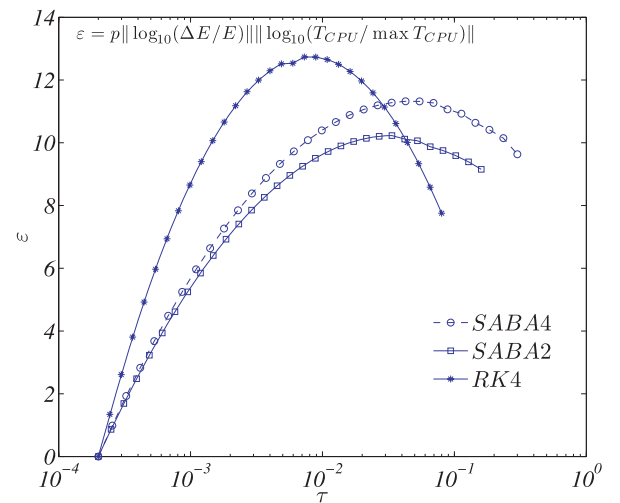


Figure 7. The efficiency $\varepsilon = p \|\log_{10}(|\Delta E/E|)\| \|\log_{10}(T_{\text{CPU}}/\max(T_{\text{CPU}}))\|$ of the global symplectic method (SABA₄ and SABA₂) and the non-symplectic one (RK4). The scales are logarithmic. See text for details.

orbits around the Sun on a circular orbit, while the third body, hereafter called the asteroid, has a negligible mass and is moving on an inner orbit ‘between’ the Sun and Jupiter. Assuming this geometry, Kozai (1962) showed that the highly inclined asteroid perturbed by Jupiter is characterized by a coupled variation in its eccentricity e and inclination i , in such a way that $H = \sqrt{a(1-e^2)} \cos(i)$ is a constant, a being the asteroid’s semimajor axis. This dynamics is often referred to as *Kozai resonance* (e.g. Libert & Henrard 2007).

It is well known that the restricted three-body problem can be reduced to 2 degrees of freedom after short-period averaging and node reduction (see for instance Malige, Robutel & Laskar 2002). Assuming that the outer giant planet is on a circular orbit, this problem becomes integrable, and its dynamics can be represented on the phase space $(e \cos \omega, e \sin \omega)$ where ω is the argument of the pericentre of the massless body (see Thomas & Morbidelli 1996; Funk et al. 2011 for more details). Such a representation is given in Fig. 8 where we have plotted several trajectories of the small body obtained by the numerical integration of the Hamiltonian equations associated to the *democratic heliocentric* formulation (see

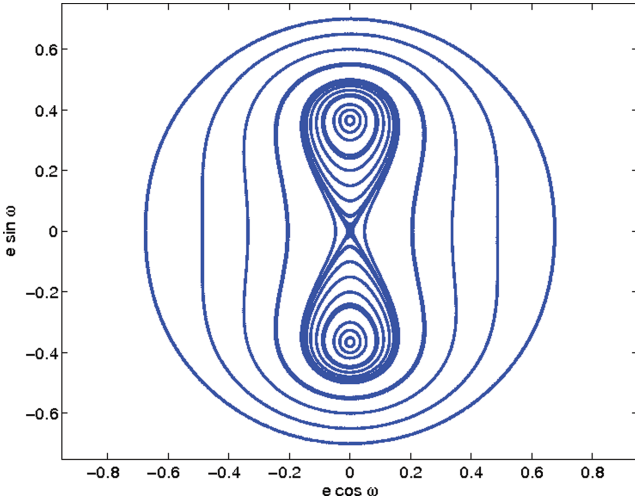


Figure 8. Restricted three-body problem phase space, corresponding to $H = 0.41833$, and reproducing the Kozai resonance (see the text for further details). Initial conditions for the calculation are the following: $a = 0.35$, $a_{\text{giant}} = 1$, $e_{\text{giant}} = 0$, $i_{\text{giant}} = 0$, where the subscript ‘giant’ refers to the outer giant planet.

for instance Duncan et al. 1998) of the three-body problem:

$$K(P_i, Q_i) = \sum_{j=1}^2 \left\{ \frac{\|P_j\|^2}{2m_j} - G \frac{m_0 m_j}{\|Q_j\|} \right\} + \frac{1}{2m_0} \left\| \sum_{j=1}^2 P_i \right\|^2 - G \sum_{j=1}^2 \sum_{i=1}^{j-1} \frac{m_i m_j}{\|Q_i - Q_j\|}. \quad (13)$$

To realize the representation of Fig. 8, we used a 10th-order SABA integrator with a sufficiently small time-step of $\tau = 10^{-3}$ yr. This phase space corresponds to $H = 0.41833$, which means a maximal inclination of 45° for the circular massless body. As one can see, for that large inclination value, circular orbit corresponds to an unstable equilibrium point (centre of the plot). A separatrix divides the phase space into three parts: two regions are characterized by the libration of ω respectively around 90° and 270° and a third one corresponding to a circulation of this angle. The two stable equilibria enclosed by the separatrix are referred to as Kozai equilibria. Hence, a massless body initially on a circular orbit will suffer large variations in eccentricity, since its real motion (short periods included) will stay close to the separatrix of the reduced problem.

Let us note that these perturbations on a small body at high inclination are secular, which means that they operate on extremely long time-scales ($\sim 10^4$ – 10^5 yr) compared to the annual orbital periodic variation of the bodies. Symplectic integrators are recommended for that kind of a problem, as they possess good energy conservation properties and are efficient for large time-steps. Our method for integrating symplectically the deviation vectors is then particularly suitable for the chaos determination of such a problem.

In Fig. 9, we report the results of the numerical computation of SALI with $SABA_{10}$ integrator ($\tau = 10^{-3}$ yr) for a regular orbit ($e = 0.4$, i.e. close to one of the stable Kozai equilibria) and for a chaotic orbit ($e = 0.001$ i.e. close to the unstable equilibrium). Our global symplectic integrator scheme reproduces correctly the expected characteristics of both the orbits in less than 40 000 yr.

Concerning the global behaviour of the phase space, it can be thoroughly described by resorting to a chaos indicator technique along a cross-section of the phase space (for instance let us consider the initial values along the $e \sin \omega$ axis when $e \cos \omega = 0$), and

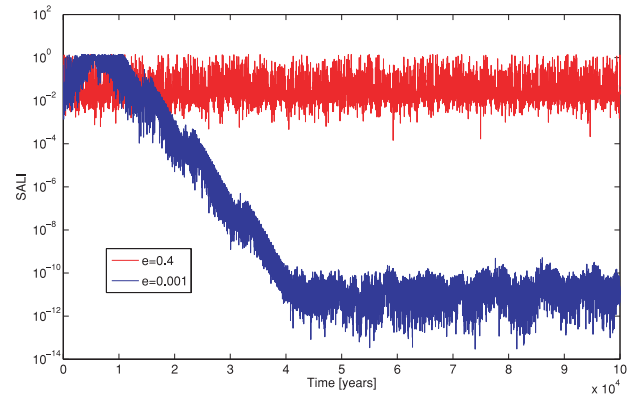


Figure 9. SALI characterization of two orbits of Fig. 8 with a symplectic $SABA_{10}$ scheme: a regular orbit at $e = 0.4$ (red) and a chaotic orbit at $e = 0.001$ (blue).

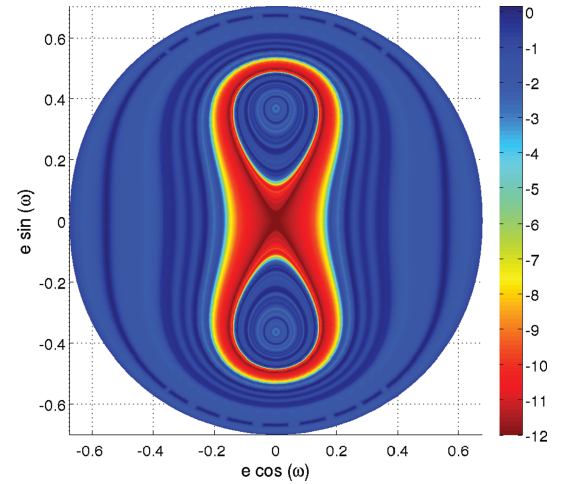


Figure 10. SALI characterization (in logarithmic scale) of the global behaviour of Fig. 8 after 100 000 yr. In order to avoid useless computation time, SALI values have been fixed to 10^{-12} when reaching this threshold. The influence of the separatrix is obvious and well identified by our symplectic $SABA_{10}$ scheme.

reporting the SALI value along the complete trajectory, as shown in Fig. 10. The chaos along the separatrix is clearly visible for values of $e \sin \omega$ close to 0 and 0.5.

In order to compare our method with a non-symplectic scheme, we have tried to reproduce these results with the Bulirsch–Stoer integration method with an accuracy parameter of 10^{-8} . The first comment is that this adaptive step-size method requires a computation time up to three times longer than the global symplectic integrator. Secondly, it appears that this non-symplectic method is unable to characterize correctly the orbits in the same integration time-span as our symplectic scheme, regardless of the time-step used. Indeed, even if the orbit is correctly described by the Bulirsch–Stoer method, the deviation vectors do not enable us to distinguish a regular behaviour from a chaotic one. To show this, we reported in Fig. 11 the norm of the same deviation vector integrated with our symplectic scheme (red curves) and with the Bulirsch–Stoer method (blue curves). Using the $SABA_{10}$ method, the norm of the deviation vector grows very rapidly for the chaotic orbit identified in Fig. 9. On the contrary, no significant deviation is observed between the two orbits of Fig. 9 for the non-symplectic method. Further calculations performed in Funk et al. (2011) showed that a Bulirsch–Stoer

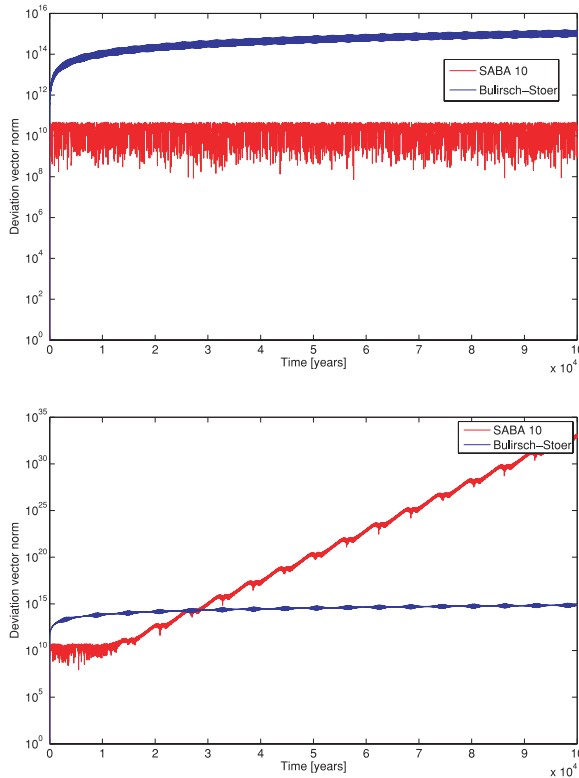


Figure 11. Norm of the deviation vector computed with $SABA_{10}$ symplectic scheme (red curves) and the Bulirsch–Stoer method (blue curves) for the two orbits of Fig. 9.

integration with accuracy parameter of 10^{-12} and a longer time-span of $\sim 10^6$ yr are required to eventually reveal the chaotic behaviour of one of these two orbits, which of course increases considerably the CPU time of the calculation. As a result, our Global Symplectic Integrator proves its efficiency in stability studies of problems of celestial mechanics.

6 CONCLUSIONS

In this work, we proposed a general method for the detection of regular and chaotic orbits in Hamiltonian systems, based on the integration of the deviation vectors used in chaos detection techniques, using symplectic algorithms. Our method has been tested on two well-known models, and the results clearly demonstrate that it outperforms non-symplectic ones.

Concerning the Hénon–Heiles system, it appears that, for large time-steps, non-symplectic integrators tend to detect an excessive number of chaotic orbits, while the global symplectic integrator is able to identify correctly the characteristics of nearly all orbits for larger time-steps, up to four times larger than the non-symplectic ones. Moreover, due to his symplectic properties, we showed that our method ensures a very small energy loss even on very long time-spans. Let us emphasize that the use of larger time-steps saves a considerable amount of computation time.

This use of larger time-steps turns out to be essential to the study of the Kozai resonance in the restricted three-body problem, where the secular orbital changes operate on extremely long time-scales. Once again, the influence of the separatrix of this problem is well identified by our global symplectic integrator. On the contrary, the Bulirsch–Stoer non-symplectic method seems unable to distinguish between regular and chaotic motion, on the same integration time-

span. A possible reason for this behaviour could be the accumulation of numerical errors introduced by the integrator and a significant energy loss, disadvantages which are avoided using our symplectic scheme.

Let us note that the choices of the $SABA$ symplectic integrator and the SALI chaos detector used in this work are arbitrary and the study of their relevance is reserved for future contribution (Hubaux, Libert & Carletti 2010).

We are confident that our findings would be generic for a large class of Hamiltonian systems. Thus we encourage scientists working on chaos indicators to perform symplectic integrations of both the orbit and the deviation vectors using the global symplectic integrator, as proposed in the present work, whenever the Hamiltonian is of the form $H(\mathbf{x}) = A(\mathbf{p}) + B(\mathbf{q})$, or generically it can be divided into two parts, each one separately integrable. Computation time and reliability of the results could thus benefit a lot from this procedure, as we have clearly demonstrated above.

ACKNOWLEDGMENTS

The work of A-SL is supported by an FNRS Postdoctoral Research Fellowship. The work of ChH is supported by an FNRS PhD Fellowship. Numerical simulations were made on the local computing resources (Cluster URB-M-SYSDYN) at the University of Namur (FUNDP, Belgium). The authors want to thank Ch. Antonopoulos for his constructive suggestions that we used to improve a previous version of our work.

REFERENCES

- Benettin G., Galgani L., Giorgilli A., Strelcyn J.-M., 1980, Meccanica, 15, 9
- Boreux J., Carletti T., Skokos Ch., Vittot M., 2010, preprint (arXiv:1007.1565)
- Bourbaki N., 1972, *Eléments de Mathématiques: Groupes et Algèbres de Lie*. Hermann, Paris
- Chambers J. E., Migliorini F., 1997, BAAS, 29, 1024
- Cincotta P. M., Simó C., 2000, A&AS, 147, 205
- Duncan M. J., Levison H. F., Lee M. H., 1998, AJ, 116, 2067
- Froeschlé C., Lega E., Gonczi R., 1997, Celest. Mech. Dynamical Astron., 67, 41
- Funk B., Schwarz R., Pilat-Lohinger E., Süli Á., Dvorak R., 2008, A&A, 57, 434
- Funk B., Libert A.-S., Süli A., Pilat-Lohinger E., 2011, A&A, 526, A98
- Guzzo M., 2005, Icarus, 174, 273
- Guzzo M., Benettin G., 2001, Discrete Cont. Dynam. Syst. B, 1, 1
- Hénon M., Heiles C., 1964, AJ, 69, 73
- Hubaux Ch., Libert A.-S., Carletti T., 2010, preprint (arXiv:1011.6207)
- Kozai Y., 1962, AJ, 67, 591
- Laskar J., 1993, Phys. D, 67, 257
- Laskar J., Robutel Ph., 2001, Celest. Mech., 80, 39
- Laskar J., Froeschlé C., Celletti A., 1992, Phys. D, 56, 253
- Levison H. F., Duncan M. J., 1994, Icarus, 108, 18
- Libert A.-S., Henrard J., 2007, Icarus, 191, 469
- Libert A.-S., Henrard J., 2008, Celest. Mech. Dynamical Astron., 100, 209
- Libert A.-S., Tsiganis K., 2009, A&A, 493, 677
- McArthur B. E., Benedict G. F., Barnes R., Martioli E., Korzennik S., Nelan E., Butler R. P., 2010, ApJ, 715, 1203
- Malige F., Robutel P., Laskar J., 2002, Celest. Mech. Dynam. Astron., 84, 283
- Manos T., Athanassoula E., 2005, in Caloli F., Contini T., Hameury J. M., Pagani L., eds, Proc. Semaine de l’ Astrophys. Française Journées de la SF2A. EDP Sciences, Les Ulis, p. 631
- Menou K., Tabachnik S., 2003, AJ, 583, 473

- Michtchenko T. A., Ferraz-Mello S., Beaugé C., 2006, *Icarus*, 181, 555
 Mikkola S., Innanen K., 1999, *Celest. Mech. Dynam. Astron.*, 74, 59
 Sándor Zs., Süli Á., Érdi B., Pilat-Lohinger E., Dvorak R., 2007, *MNRAS*, 375, 1495
 Skokos Ch., 2001, *J. Phys. A*, 34, 10029
 Skokos Ch., Gerlach E., 2010, *Phys. Rev. E*, 82, 036704
 Skokos Ch., Antonopoulos Ch., Bountis T. C., Vrahatis M. N., 2004, *J. Phys. A*, 37, 6269

- Skokos Ch., Bountis T., Antonopoulos Ch., 2007, *Phys. D*, 231, 30
 Széll A., Érdi B., Sándor Zs., Steves B., 2004, *MNRAS*, 347, 380
 Thomas F., Morbidelli A., 1996, *Celest. Mech. Dynam. Astron.*, 64, 209
 Wisdom J., Holman M., 1991, *AJ*, 102, 1528

This paper has been typeset from a $\text{\TeX}/\text{\LaTeX}$ file prepared by the author.